Proceedings of the 2023
30th International Conference on Nuclear Engineering
ICONE30
May 21-26, 2023, Kyoto, Japan

ICONE30-1681

ASSESSMENT OF CFD CODES CAPABILITIES TO PREDICT THE RISK OF FLAMMABILITY OR EXPLOSIVITY IN THE EVENT OF A HYDROGEN LEAK IN NUCLEAR FACILITIES

Thomas Gélain, Corinne Prévost and Nadia Liatimi
Institut de Radioprotection et de Sûreté Nucléaire (IRSN), PSN-RES, SCA,
Gif-Sur-Yvette, 91192, France

ABSTRACT

In the context of nuclear safety, a 4 m^3 experimental ventilated enclosure called CARDAMOMETTE has been implemented at IRSN to study the risk of explosion in the event of a hydrogen leakage from a duct in a nuclear facility. Different configurations of hydrogen leakage have been studied allowing to identify those that could potentially lead to explosivity conditions. For safety reason, helium was considered to simulate the behavior of hydrogen. Thanks to high level instrumentation (PIV, He mass spectrometry) and a well-equipped facility allowing local measurements inside the enclosure, a lot of data has been acquired, ensuring a very accurate validation of the CFD code ANSYS CFX. The objective of this validation is to evaluate the capabilities of the CFD code to predict the potential risk of explosivity depending on gas leakage and ventilation configurations.

For this purpose, an experimental and numerical program has been launched to study the influence of ventilation (location of air inlets, renewal rates), gas leakage configurations (location and flowrate, impinging jet) and space clutter (cylindrical container, tubes network, suspended ceiling) on helium dispersion inside the experimental bench and to highlight those leading to hazardous situations.

First, code-experiment comparisons of airflows inside the enclosure were led to ensure the capability of the CFD code to reproduce experimental airflows for some configurations. PIV velocity fields and experimental air renewal curves have been compared to those obtained with CFD calculations, showing a satisfactory agreement. Thanks to this first step, optimal numerical parameters (turbulence model, mesh, boundary conditions) have been chosen.

Secondly, studies of helium dispersion were carried out according to the different configurations presented before. In this paper, only results for free helium jet and impinging helium jet on the wall are presented. Experimental and numerical results of local concentrations were compared, showing a very good agreement and hence the capability of the code to highlight the high concentration areas. Sensitivity studies about turbulent Schmidt number were also led, allowing to define the best numerical dataset depending on the helium injection configurations.

Other experimental and numerical comparisons are currently in progress, especially for the configuration of an impinging helium jet on a cylindrical container.

Keywords: Hydrogen, CFD, Dispersion, nuclear facility, explosivity

NOMENCLATURE

Latin letters

g	gravity ($m.s^{-2}$)
k	turbulent kinetic energy ($m^2.s^{-2}$)
M	gaseous mixture molar mass ($kg.mol^{-1}$)
$\overline{P}$	average pressure (Pa)
R	perfect gas constant ($J.mol^{-1}.K^{-1}$)
S_i	mass fraction source term for species i ($kg.m^{-3}.s^{-1}$)
t	time (s)
T	temperature (K)
$\overline{U}$	average component of velocity vector ($m.s^{-1}$)
u^*	friction velocity ($m.s^{-1}$)
Y_i	mass fraction for species i (-)

Greek letters

Γ_i	molecular diffusion coefficient for species i ($m^2.s^{-1}$)
$\Gamma_{eff,i}$	effective diffusivity for species i ($m^2.s^{-1}$)
ρ	gaseous mixture density ($kg.m^{-3}$)
σ_t	turbulent Schmidt number (-)
μ	gaseous mixture dynamic viscosity (Pa.s)
μ_t, μ_{eff}	turbulent and effective dynamic viscosity (Pa.s)

© 2023 by JSME

1. INTRODUCTION

In the frame of safety of nuclear facilities, the release of hydrogen in the event of an accident is one of the most dreaded scenarios, which may lead to an ignition or an explosion if hydrogen level is sufficient and ambient conditions are favorable [1]. Examples of such accidents are unfortunately well-known, namely Three Mile Island in 1979, Chernobyl in 1986 and more recently Fukushima Daiichi in 2011. These severe accidents concerned Nuclear Power Plants and are due to the reaction between steam and zirconium which generates hydrogen.

But hydrogen (gas or liquid) is also frequently used in other nuclear facilities (nuclear laboratory and factory), for example in the step of conversion of Uranium Oxide, and also in many non-nuclear industrial activities [2] like aerospace [3], metallurgy [4], maritime [5], ammonia production [6], pharmaceuticals [7], automotive [8], and other fields with large-scale hydrogen production. So its storage or its transport by pipe may potentially lead to hydrogen leak and release into a building or a tunnel [2] [9] [10] with the consequences reminded above. It is reminded that for a hydrogen volume concentration upper than 4 % (Lower Flammability Limit LFL), the mixture air-hydrogen may ignite and upper than 13 % (Lower Explosivity Limit LEL) [1], it may detonate

In the context of safety assessment of nuclear facilities (except severe accident in a power plant), this type of incident has been studied by the way of risk analysis [11] or research studies which interest especially to the density effects [12] or to specific configurations which may lead to a local accumulation of gas and to a risk of flammability or explosivity [13].

This article focuses on the experimental and numerical study of hydrogen injection configurations in a ventilated analytical enclosure which may lead to situations for which local hydrogen concentration reaches the low flammability level of 4 %. This study is a continuation of previous ones [12] [14], but at a very analytical level based on a well-instrumented facility (PIV, mass spectrometry, multiple sampling points) dedicated to providing global and local data of concentration and velocity to validate CFD codes.

2. MATERIALS AND METHODS

This section details the experimental facility, called CARDAMOMETTE, implemented to study the dispersion of a light gas (helium) which is commonly used to simulate hydrogen without explosion hazard. It also presents numerical simulations with ANSYS CFX devoted to reproducing experiments in CARDAMOMETTE and to validate the CFD code for specific scenarios and to be able to predict the dispersion of hydrogen in other situations representative of accidental scenarios which could occur in industrial facilities.

2.1. Experimental Setup

Experiments were led in CARDAMOMETTE enclosure, the dimensions of which are reminded in Figure 1.

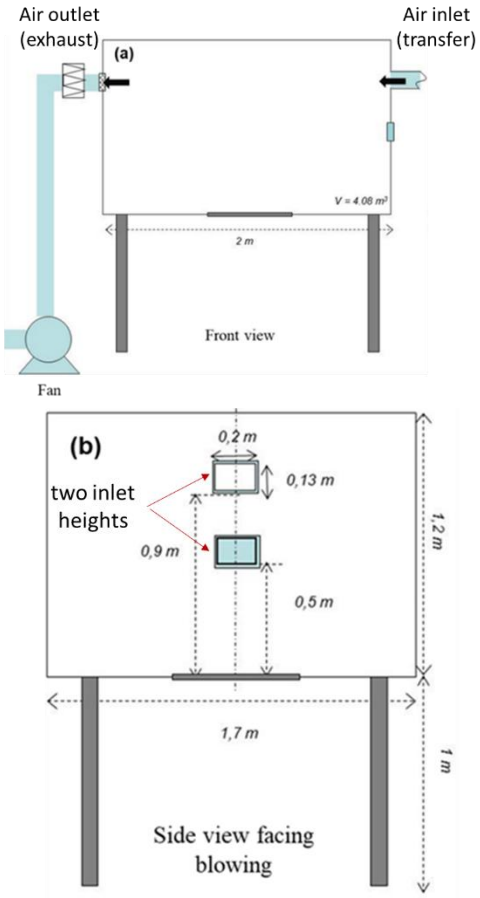

FIGURE 1: FRONT (a) AND SIDE (b) VIEWS AND DIMENSIONS OF CARDAMOMETTE ENCLOSURE

CARDAMOMETTE is composed of an enclosure of 2 m length, 1.7 m width and 1.2 m height for a volume of 4.08 m^3. Two openings are located on the two smallest sides face-to-face at 0.9 m height for the extraction (outlet) and at 0.9 m or 0.5 m height for the transfer opening (inlet) depending on the chosen scenario; for the present paper, transfer opening is located at 0.5 m. Their dimensions are 0.13 m height and 0.2 m width.

A rectangular pipe of 0.8 m length is located upstream the transfer opening to avoid edge effect at the enclosure entrance.

2.2. Measurement methods

This experiment is dedicated to the study of helium dispersion in the ventilated enclosure. To well understand the behavior of helium gas inside the enclosure, it is essential to characterize the airflows which will probably control its dispersion. For that, a PIV system was implemented in the facility to visualize the airflows and to measure the velocities fields induced by the blowing jet and by the helium jet which may also influence the airflows and its distribution inside the enclosure.

Hence, measurement in horizontal and vertical planes with different sizes were considered to apply PIV for airflows characterization.

© 2023 by JSME

For helium concentration measurement, mass spectrometers were used with a sampling probe which was located at different locations inside the enclosure. For that, the facility was equipped with four pillars (Figure 2) distributed inside the enclosure, allowing to get a lot of helium concentration data at different heights. For each pillar, at least 3 sampling points (Low, Median and High) are available and for pillars A and C, a motorized rail allows to get concentration at several heights distributed along the pillar.

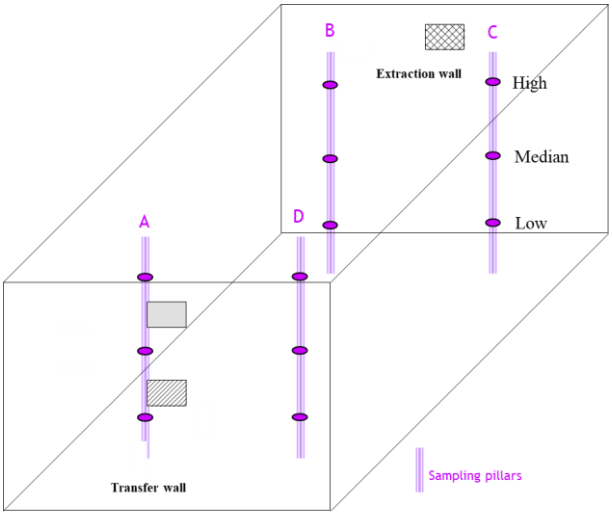

FIGURE 2: PILLARS LOCATION INSIDE CARDAMOMETTE ENCLOSURE

These numerous data are needed to highlight a potential local overconcentration of helium and to allow an accurate validation of the CFD code.

2.3. Experimental tests

Three scenarios of helium injection have been planned to study different configurations:

- the first one was a free helium jet oriented towards the transfer wall (figure 3);
- the two others were helium jets impacting the transfer wall (figure 4) for two wall distances, 30 cm and 10 cm.

The experimental scenario consisted of the two following steps: ventilation of the enclosure during a sufficient renewal time to establish the flow inside the enclosure, then injection of helium gas with a continuous mass flowrate up to reach a state of equilibrium of concentrations in the overall enclosure and in the extraction duct which is representative of the global concentration.

The parameters of the 3 tests are reminded in table 1.

TABLE 1: CONFIGURATION PARAMETERS

Tests	$Q_{extraction}$	d_{inj}	Q_{he}
Free helium injection	59 $m^3.h^{-1}$	4 mm	2.69 $m^3.h^{-1}$
Impacting helium jet (30 cm)			
Impacting helium jet (10 cm)			

It may be noticed that for a volume flowrate $Q_{extraction}$ = 59 $m^3.h^{-1}$ and a volume of enclosure V = 4.08 m^3, the theoretical renewal rate of CARDAMOMETTE is $R = {Q_{extraction}}/{V} = 14.5\ h^{-1}$ and the renewal time of the enclosure is $t_R = {3600}/{R} \approx 250\ s$. Hence, the minimum time to reach the equilibrium concentration of helium may be estimated to 4 x t_R = 1000 s. So, all the experimental and numerical tests had a duration of at least 1000 s for the gas injection phase.

During the injection phase, helium concentration was continuously measured at some points and, when the concentration equilibrium was reached, all points distributed on the pillars were monitored to get concentration data to compare with numerical results.

2.4. Numerical simulations

- Basic equations

Numerical simulations of airflows and helium dispersion in the ventilated enclosure were performed with the CFD code ANSYS CFX version 21.

The equations solved in the calculations performed with CFX are based on some assumptions: the fluid considered is an air/helium mixture, taken to be mixed at the molecular level (multi-species formulation). The flow is turbulent, isothermal (25°C) and weakly compressible. The gaseous mixture is assumed to be an ideal gas; consequently, the density ρ of the gaseous mixture is given by the ideal gas equation of state (Eq. 1).

$$\rho = \frac{\bar{P}M}{RT} \qquad with \qquad \frac{1}{M} = \sum_{c=1}^{n} \frac{\bar{Y}_c}{M_c} \tag{1}$$

where P is the pressure (Pa), M is the molar weight ($kg.mol^{-1}$), R is the constant of ideal gas ($J.mol^{-1}.K^{-1}$) and T is the temperature (K). Before the helium injection, the flow is taken to be established, and for this an initial stationary calculation is performed, followed by a second transient calculation of helium injection for a given time. The flows are simulated by solving the non-stationary Navier–Stokes equations with turbulence using the standard RANS (Reynolds Averaged Navier Stokes) approach described below. We note that in the special case of the stationary calculation performed before the helium injection, all the transient terms appearing in the non-stationary equations are zero.

$$\frac{\partial \rho}{\partial t} + \nabla.(\rho \bar{U}) = 0 \tag{2}$$

$$\frac{\partial \rho \bar{U}}{\partial t} + \nabla.(\rho \bar{U} \otimes \bar{U}) = -\nabla \bar{\bar{P}} + \nabla\left[\mu_{eff}(\nabla \bar{U} + (\nabla \bar{U})^T)\right] + \rho g \tag{3}$$

where $\mu_{eff} = \mu + \mu_t$ and $\bar{\bar{P}} = \bar{P} + \frac{2}{3}\rho k$.

© 2023 by JSME

The turbulent viscosity μ_t is calculated using a k-ω SST (Shear Stress Transport) first-order model of turbulence which was chosen after a turbulence model sensitivity study.

- Transport equation

The calculations carried out with CFX consist in simulating the dispersion of helium in the CARDAMOMETTE ventilated enclosure. Two gases, air and helium, are considered but only helium transport is simulated, the mass fraction of air being calculated as the difference (Eq. 5). The transport of the mass fraction of helium Y_{he} is governed by Eq. 4:

$$\frac{\partial \rho \bar{Y}_{he}}{\partial t} + \nabla.(\rho \bar{U} \bar{Y}_{he}) = \nabla\left[\Gamma_{he_{eff}} \nabla \bar{Y}_{he}\right] + S_{he} \quad (4)$$

$$\bar{Y}_{air} = 1 - \bar{Y}_{he} \quad (5)$$

where $\Gamma_{he_{eff}} = \Gamma_{he} + \frac{\mu_t}{\sigma_t}$, and σ_t is the turbulent Schmidt number (default value is 1 in Ansys CFX).

- Preprocessing (geometry, mesh and dataset)

Based on the design presented in figure 1, a geometry of CARDAMOMETTE was made as computational domain. It is presented in figure 3 and it is the most representative of the real enclosure. It may be noticed that the transfer opening is in the configuration of low position (0.5 m height).

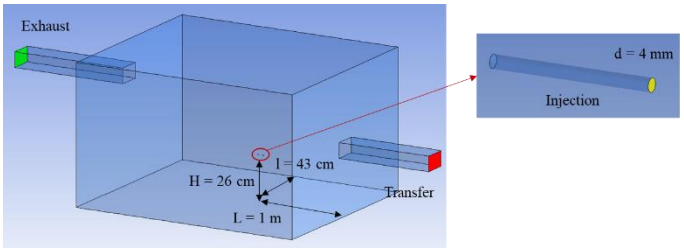

FIGURE 3: GEOMETRY OF CARDAMOMETTE ENCLOSURE WITH FREE HELIUM JET

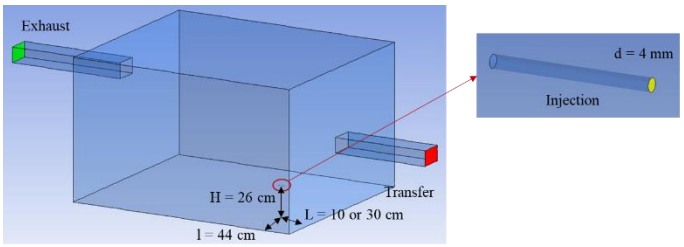

FIGURE 4: GEOMETRY OF CARDAMOMETTE ENCLOSURE WITH IMPACTING HELIUM JET

Both figures 3 and 4 show the geometry of the enclosure with its normal ventilation configuration as well as the injection configurations detailed in chapter 2.3. The injection is modelled with a small duct of 10 cm length and a diameter of 4 mm.

The geometries were then meshed to be implemented in the dataset and meshes are shown in figures 5 and 6. A method of influence sphere was applied to mesh the trajectory of helium jet allowing a good representation of helium dispersion close to the injection. Furthermore, a thin mesh was also done to get accuracy enough for helium concentration inside the enclosure and to allow an efficient comparison with experimental data.

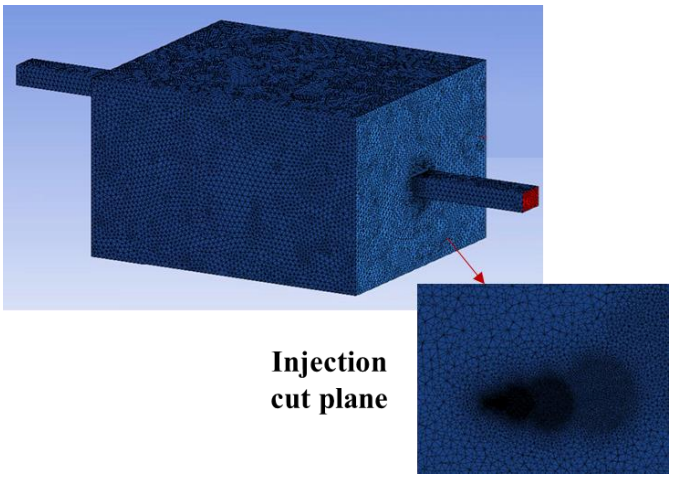

FIGURE 5: MESH OF CARDAMOMETTE ENCLOSURE WITH FREE HELIUM JET

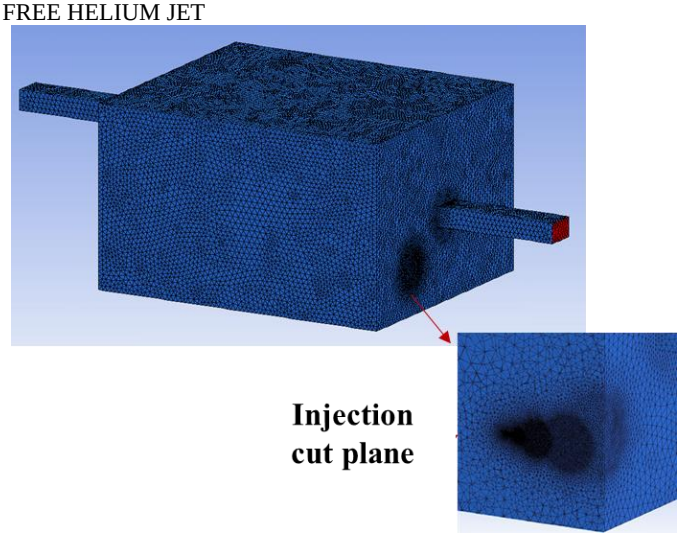

FIGURE 6: MESH OF CARDAMOMETTE ENCLOSURE WITH IMPACTING HELIUM JET

The mesh parameters applied to the geometries presented in figure 3 and figure 4 are reminded in table 2.

TABLE 2: MESH PARAMETERS FOR ALL INJECTION CONFIGURATIONS

Parameters	Free jet	Impacting jet (30 cm)	Impacting jet (10 cm)
Min size (mm)	0.3		
Max size (cm)	4		
Mean size (cm)	3		
Number of elements	4 084 840	3 815 945	3 539 765

© 2023 by JSME

When the mesh was done, it was implemented in the dataset into which numerical parameters and input data (boundary conditions) were defined. Numerical parameters are detailed in table 3. It may be noticed that the turbulence model and the discretization scheme have been chosen following sensitivity studies. For the turbulence model, k-ω SST gives better results than k-ε and RSM models in terms of concentration levels and for the discretization scheme, HRS strongly improves concentration tine evolutions compared to the upwind scheme.

TABLE 3: NUMERICAL PARAMETERS

Parameters	ANSYS CFX
Regime	Transient
Timestep	Progressive from 0.1 s to 2 s
Turbulence model	k-ω SST
	Variable Schmidt number from 0.3 to 1
Discretization scheme	High Resolution Scheme (HRS - 1st/2nd order auto)

The parameters applied to all boundary conditions (BCs – Figure 6) are presented in table 4.

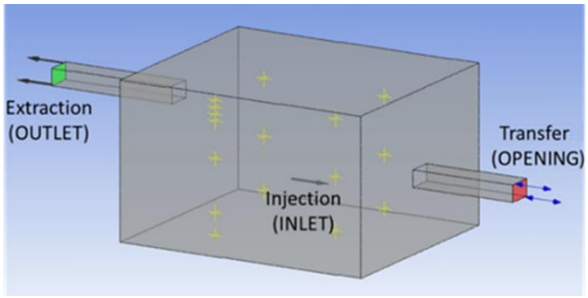

FIGURE 6: BOUNDARY CONDITIONS

TABLE 4: BCs and INPUT DATA

Condition	Paramètres
Transfer **(in red in figure 6)**	**Opening (free flow)** $P_{rel} = 0$ Pa
Extraction **(in green in figure 6)**	**Outlet (imposed outlet with mass flowrate)** $Q_s = 59\ m^3.h^{-1}$, $q_s = 0{,}0197\ kg.s^{-1}$ $k = \frac{3}{2}(I\,U)^2$, $\varepsilon = C_\mu \rho \frac{k^2}{\mu_t}\ m^2.s^{-3}$, $\omega = \frac{\varepsilon}{k}$ $\mu_t = 1000 I\mu$ ($I = 3{,}7\%$) $Y_{he} = 0$
Injection	**Inlet (imposed inlet with mass flowrate)** $Q_{inj} = 2{,}69\ m^3.h^{-1}$, $q_{inj} = 0{,}000124\ kg.s^{-1}$ $k = \frac{3}{2}(I\,U)^2$, $\varepsilon = C_\mu \rho \frac{k^2}{\mu_t}$, $\omega = \frac{\varepsilon}{k}$ $\mu_t = 1000 I\mu$ ($I = 3{,}7\%$) $Y_{he} = 1$
Walls	**Wall** No slip conditions Automatic wall law

3. RESULTS AND DISCUSSIONS

Experimental and numerical results are compared in terms of helium jet velocity profiles and helium concentration.

3.1. Velocity results

Thanks to PIV measurements, different profiles of velocities were acquired to characterize the behavior of helium, especially close to the wall. Their location is shown in figure 7, but only some of them will be presented in this paper.

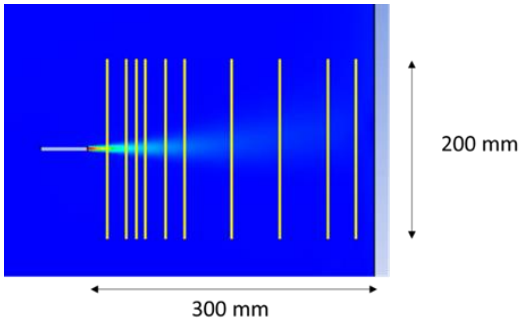

FIGURE 7: JET VELOCITY PROFILES LOCATION

PIV results are presented in figures 8 (visualization and velocity fields) and 9 (velocity profiles) at different distances from the injection nozzle for the case of a jet impact distance of 30 cm. It may be noticed that PIV measurements close to the wall are complicated due to reflections of the laser beam with the wall; that is why the uncertainty are more important when the velocity profiles are closer to the wall.

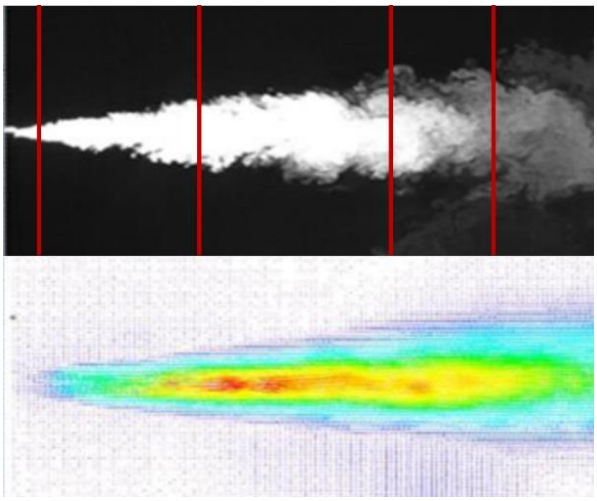

FIGURE 8: VISUALIZATION OF HELIUM JET AND PIV MEASUREMENT WITH EXTRACTED VELOCITY PROFILES AT DIFFERENT DISTANCES FROM THE INJECTION NOZZLE

© 2023 by JSME

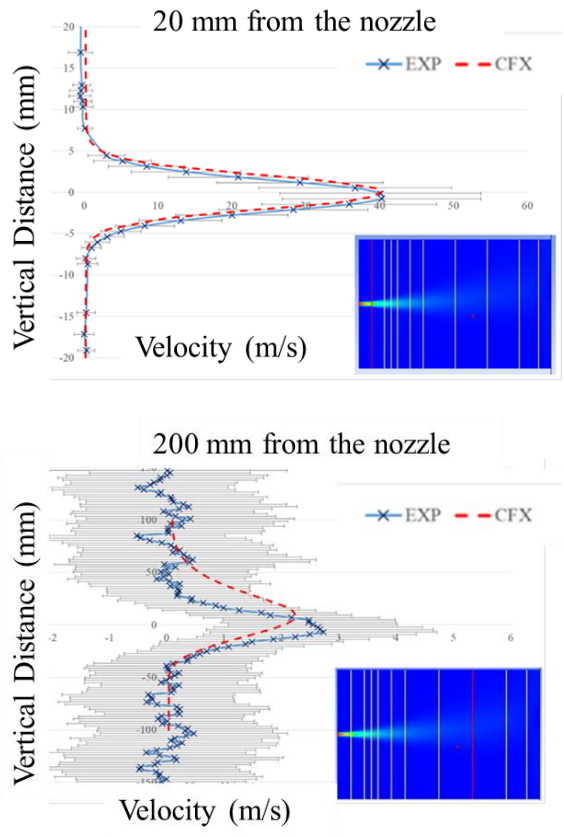

FIGURE 9: EXPERIMENTAL AND NUMERICAL VELOCITY PROFILES IN THE HELIUM JET AT 20 MM AND 200 MM FROM THE INJECTION NOZZLE

The results presented in figure 9 show a satisfactory agreement between numerical and experimental results. For the first profiles at 20 mm, experimental (EXP) and numerical (CFX) results are both overlapped; for the profiles at 200 mm, there is a slight difference between them, but velocity level is similar and, given the experimental uncertainties, the agreement is acceptable.

Similar comparisons were made for free helium jet and impacting jet at 10 cm with the same agreement, but they are not presented in this paper.

So, these first results show the capabilities of the CFD code to reproduce helium jet trajectory even near the wall. Following that, experimental and numerical helium concentrations were compared for the three injection cases and are presented thereafter.

3.2. Transient concentration results

First, time evolutions of helium concentration for some measurement points are presented in figure 10.

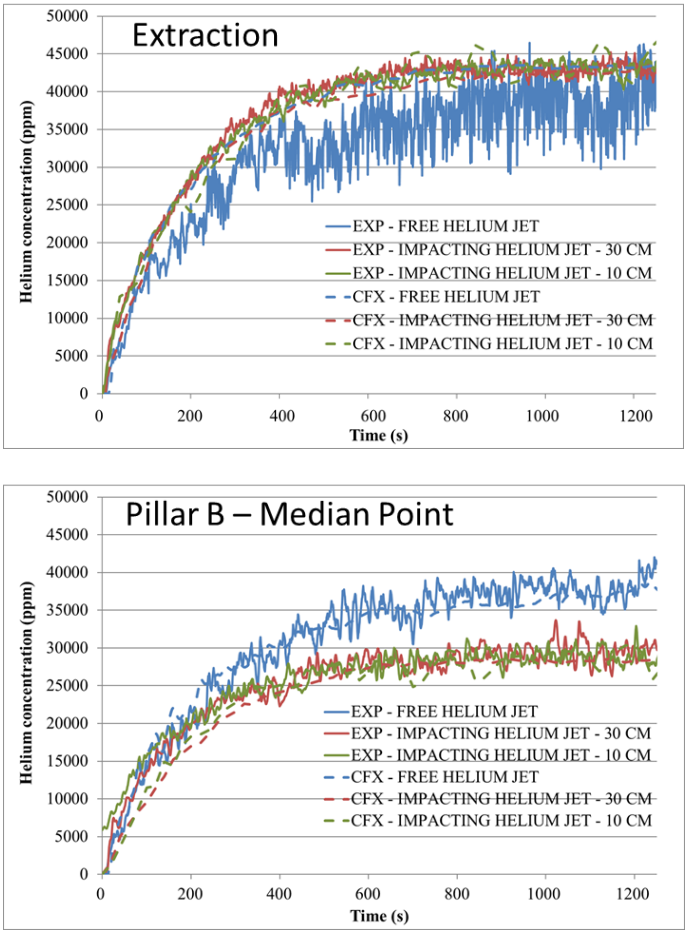

FIGURE 10: EXPERIMENTAL AND NUMERICAL COMPARISON OF TIME EVOLUTION OF HELIUM CONCENTRATION AT EXTRACTION AND PILLAR B MEDIAN POINT

The comparison presented in figure 10 shows a very good agreement between experimental and numerical results for both locations in the enclosure, extraction and median point of pillar B. The CFD code correctly reproduces the time evolution of the concentration and can calculate the levels of equilibrium concentration for free helium injection and impacting helium injection at 10 and 30 cm.

3.3. Equilibrium concentration results

Different points were then monitored at the equilibrium of the concentration: all points Low, Median and High for each pillar and several points on the pillars equipped with a motorized rail (pillars A, B or C depending on the injection configuration).

- Free helium jet results

Figure 11 presents a numerical field of helium concentration inside the enclosure at the equilibrium state. As it can be seen, a stratification is established due to the density of helium which is around 7 times lower than the air density.

© 2023 by JSME

Given the color scale, the maximal level of concentration inside the enclosure seems to reach the lower inflammability limit of 4 % mentioned in introduction from a certain height inside the enclosure and close to the emission source.

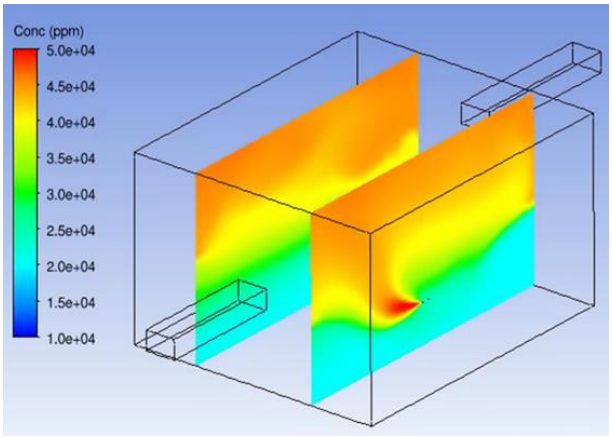

FIGURE 11: NUMERICAL FIELD OF HELIUM CONCENTRATION INSIDE THE ENCLOSURE (FREE HELIUM INJECTION)

Following this result, a comparison between experimental and numerical concentrations at the sampling points was made and is presented on three graphs in figure 12, each one related to the point located at a specific level inside the enclosure (High, Median and Low).

All numerical results are presented for 3 values of turbulent Schmidt number σt (0.3 – 0.5 – 0.7), knowing that this parameter may influence the distribution of helium inside the enclosure.

So, a sensitivity study is presented for each kind of helium injection to optimize this value and to understand its influence depending on the configuration.

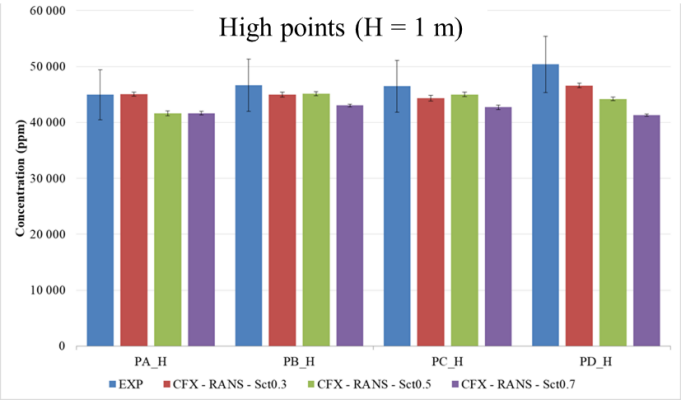

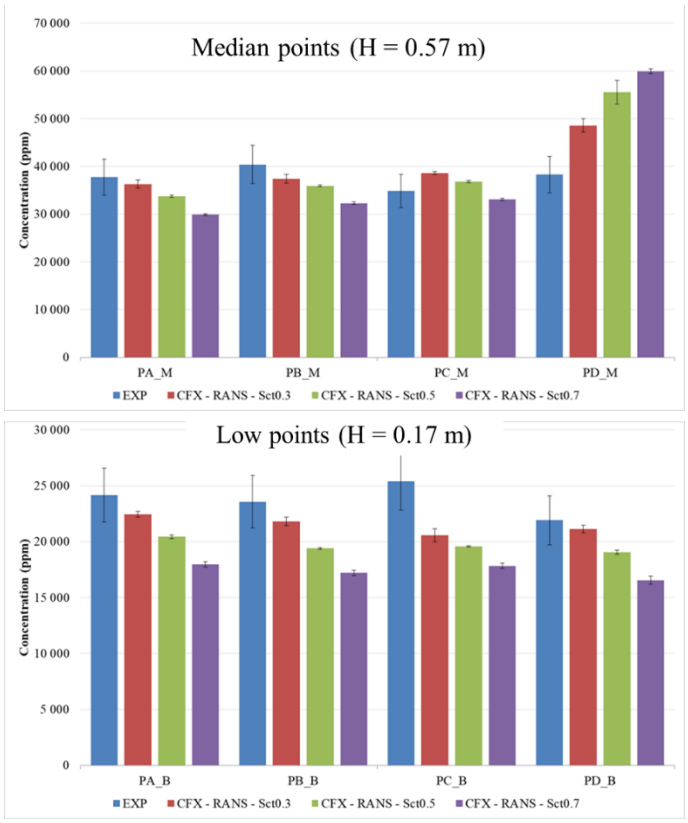

FIGURE 12: EXPERIMENTAL AND NUMERICAL CONCENTRATION RESULTS AT HIGH, MEDIAN AND LOW LEVEL POINTS (FREE HELIUM INJECTION)

The results presented in figure 12 show a good agreement between experimental and numerical concentrations whatever the studied level. It may be stated that for the High level, average concentration is around 45 000 ppm (4.5 % > LFL), for Median level it is around 35 000 ppm (3,5 %) and for Low level, it is less than 25 000 ppm (2,5 %). These results are relevant with figure 11. It may be also noticed the sensitivity of the results to the turbulent Schmidt number which shows that the lowest value of 0.3 allows to get the results closest to experimental ones. This influence may be explained because the turbulent Schmidt number is present in the helium mass fraction transport equation (eq. 5) and more precisely in helium diffusivity as reminded thereafter:

$$\Gamma_{he_{eff}} = \Gamma_{he} + \frac{\mu_t}{\sigma_t} \qquad (6)$$

Hence, the lower the turbulent Schmidt number, the higher the helium diffusivity. However, the influence of this parameter is also related to the strength of helium jet compared to ambient airflows as illustrated in the following results.

- Impacting helium jet results (30 cm)

The results for impacting helium jet at 30 cm from the wall are presented below. Figure 13 shows helium concentration

© 2023 by JSME

fields inside the enclosure at equilibrium state and highlights a stratification with a maximal level of concentration slightly higher than for the free helium jet.

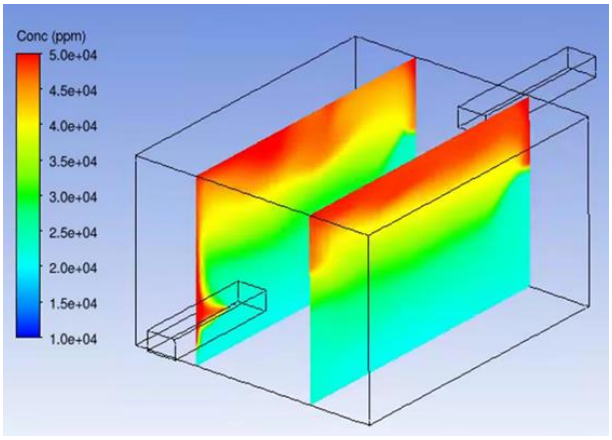

FIGURE 13: NUMERICAL FIELD OF HELIUM CONCENTRATION INSIDE THE ENCLOSURE (IMPACTING HELIUM INJECTION – 30 CM)

Results of helium concentration are then presented for High, Median and Low levels points in figure 14. It may be observed that for each level, the concentration is homogeneous with a concentration value of around 45 000 ppm for High level points (> LFL), around 27 000 ppm for Median level points and around 22 000 ppm for Low level points.

As it can be seen in figure 14, CFD results are in good agreement with experimental ones for all points. Regarding the influence of turbulent Schmidt number on concentration distribution, it may be stated that for the configuration of impacting helium jet, unlike free helium jet configuration, helium concentration results are poorly sensitive to this value.

The reason is that the helium jet loses a lot of momentum when it impacts the wall and does not influence the airflows inside the enclosure. Hence, helium distribution is more induced by the airflows from the ventilation than by helium jet. For free helium jet configuration, the jet of gas is not disturbed and its strong velocity at nozzle output (around 70 m/s) will influence the airflows inside the enclosure and helium distribution inside the enclosure.

To summarize:

- for free helium jet configuration, helium jet drives the airflows inside the enclosure and thus helium distribution is sensitive to turbulent Schmidt number modification;
- for impacting jet configuration, helium jet does not drive the airflows inside the enclosure and thus helium distribution is lowly sensitive to turbulent Schmidt number modification.

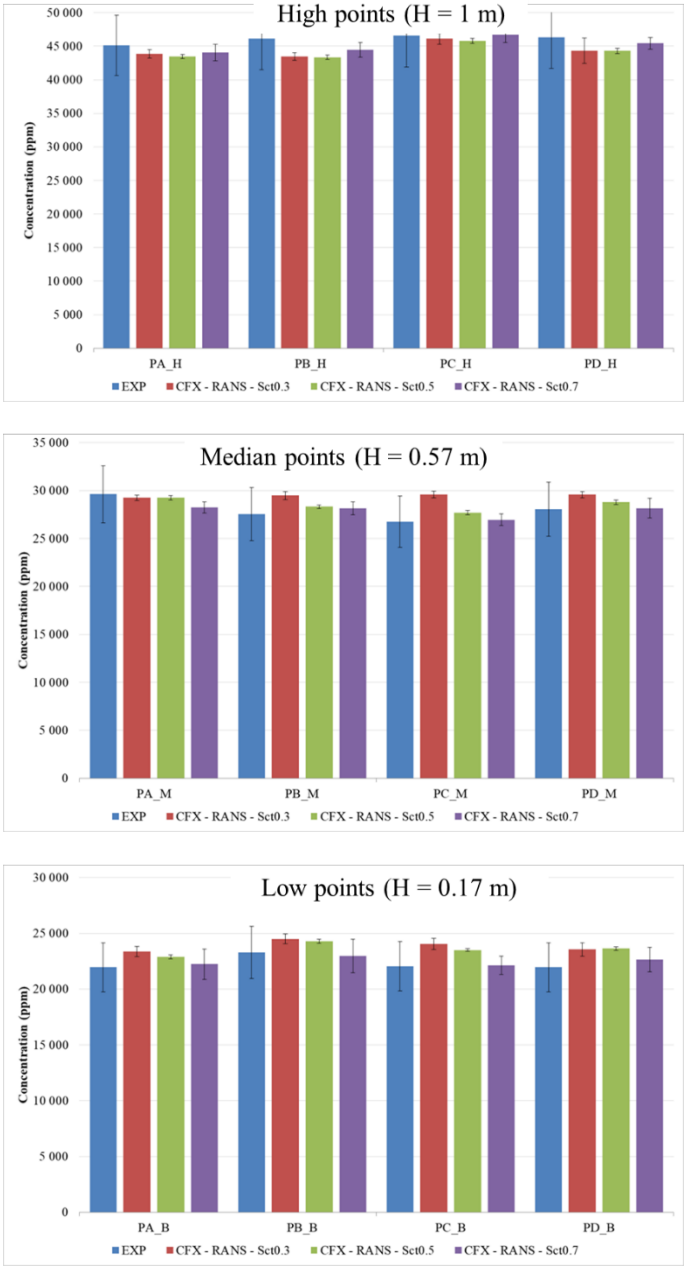

FIGURE 14: EXPERIMENTAL AND NUMERICAL CONCENTRATION RESULTS AT HIGH, MEDIAN AND LOW LEVELS POINTS (IMPACTING HELIUM INJECTION – 30 CM)

Following the study of impacting helium jet at 30 cm, a similar study was also led for an impacting helium jet at 10 cm. The results are not presented here because they are quite similar to those at 30 cm. However, these results are considered in the next summary.

© 2023 by JSME

- Summary

To summarize all results acquired for this experimental and numerical study, figure 15 presents three graphs of helium concentration at all points monitored experimentally for each configuration.

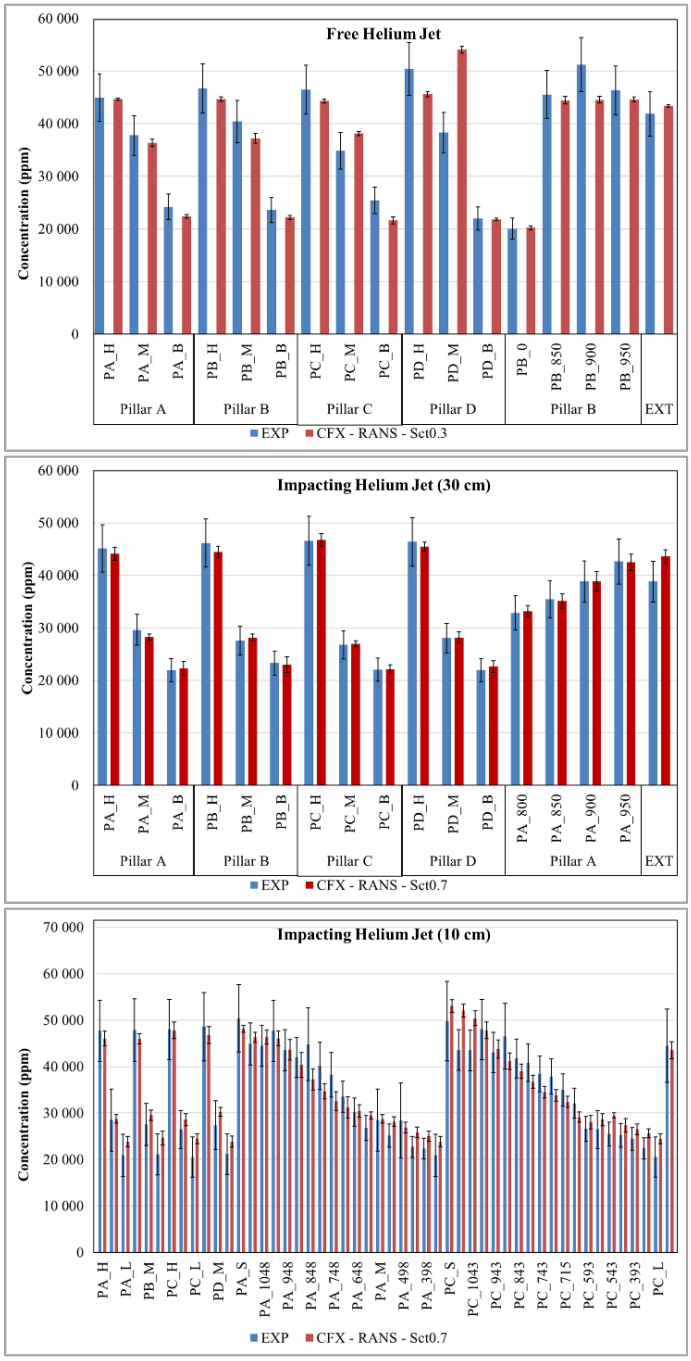

FIGURE 15: HELIUM CONCENTRATION RESULTS SUMMARY FOR EACH HELIUM JET CONFIGURATION

Figure 15 presents a summary of the results obtained for each helium jet configuration. For all graphs, PA, PB, PC and PD mean Pillar A, B, C and D, and the letter H, B, M and S respectively means High, Low, Median and Ceiling. EXT corresponds to the average concentration sampled in the extraction duct. For the points associated to a number, the latter corresponds to the height (in mm) of the point from the floor at the corresponding pillar in the enclosure.

As seen in figure 15, the comparison between experimental and numerical is quite good for all points considering experimental uncertainties; the CFD code is able, first to reproduce the stratification inside the enclosure whatever the studied injection configuration, and second to calculate the good level of concentration.

To quantify this agreement between both experimental and numerical results, the average relative difference between them is calculated in table 5.

TABLE 5: RELATIVE DIFFERENCE BETWEEN NUMERICAL AND EXPERIMENTAL HELIUM CONCENTRATION

	Free jet	Impacting jet 30 cm	Impacting jet 10 cm
More relevant σ_t	**7.4 %**	**2.2 %**	**8.5 %**
Less relevant σ_t	*18.1 %*	*5.2 %*	*10.4 %*

In table 5 are presented the relative differences between experimental and numerical helium concentrations for all points of each jet configuration, for the most and the less relevant turbulent Schmidt number. It may be stated that for the most relevant one, the maximal difference is 8.5 % and even for the less relevant one, the relative difference is lower than 20 %. So numerical results are very satisfactory and it may be concluded that the CFD code is able to predict with a good accuracy helium (or hydrogen) distribution in the event of an accidental leak in an industrial facility.

4. CONCLUSION

This article presents an experimental and numerical study about the dispersion of hydrogen gas, simulated by helium, in a ventilated enclosure. The objective is first to discriminate the configuration leading to local overconcentration which may exceed the Lower Flammability Limit (LFL), and second to validate the numerical tool ANSYS CFX in order to use it for other parametrical studies.

Different configurations of gas injection inside the CARDAMOMETTE enclosure were studied either for free or impacting helium jet, and several helium concentration monitoring points were acquired to compare experimental and numerical results.

The results presented in this present article show that for the studied configuration, the Lower Flammability Limit (LFL) is

© 2023 by JSME

always exceeded above a certain height inside the enclosure that could lead in the event of hydrogen leak to a potential explosion.

Furthermore, the comparison between experimental and numerical results highlights very good predictions of the CFD code whatever the studied configuration and the location of the injection place inside the enclosure. A parametrical numerical study about the turbulent Schmidt number also highlights its influence on helium concentration distribution inside the enclosure, especially for the case of free helium jet with a strong injection velocity, widely upper than blowing one.

The most relevant turbulent Schmidt number has been defined for which the average error between numerical and experimental concentrations does not exceed 8.5 % which is greatly satisfactory for the code validation.

It may be noticed that this error reaches 18.1% with the less relevant turbulent Schmidt number, but it is still satisfactory regarding experimental uncertainties.

As a conclusion, the results presented here allow to consider that the CFD code validation for the evaluation of the distribution of a hazardous gas like hydrogen in a ventilated enclosure is well advanced, but other configurations of injection or ventilation must be studied to consolidate these results and the trust that we may get into the CFD code.

REFERENCES

[1] "Safety, Codes and Standards - Basics Hydrogen and Fuel Cell Technologies Office." www.eere.energy.gov/hydrogenandfuelcells/codes.

[2] X. Tang, L. Pu, X. Shao, G. Lei, Y. Li, and X. Wang, "Dispersion behavior and safety study of liquid hydrogen leakage under different application situations," *Int. J. Hydrogen Energy*, vol. 45, no. 55, pp. 31278–31288, 2020, doi: 10.1016/j.ijhydene.2020.08.031.

[3] A. Baroutaji, T. Wilberforce, M. Ramadan, and A. G. Olabi, "Comprehensive investigation on hydrogen and fuel cell technology in the aviation and aerospace sectors," *Renew. Sustain. Energy Rev.*, vol. 106, no. September 2018, pp. 31–40, 2019, doi: 10.1016/j.rser.2019.02.022.

[4] J. Bilik, P. Pustejovska, S. Brozova, and S. Jursova, "Efficiency of hydrogen utilization in reduction processes in ferrous metallurgy," *Sci. Iran.*, vol. 20, no. 2, pp. 337–342, 2013, doi: 10.1016/j.scient.2012.12.028.

[5] C. Deniz and B. Zincir, "Environmental and economical assessment of alternative marine fuels," *J. Clean. Prod.*, vol. 113, no. X, pp. 438–449, 2016, doi: 10.1016/j.jclepro.2015.11.089.

[6] K. R. Tolod, S. Hernández, E. A. Quadrelli, and N. Russo, "Chapter 4 - Visible Light-Driven Catalysts for Water Oxidation: Towards Solar Fuel Biorefineries," in *Horizons in Sustainable Industrial Chemistry and Catalysis*, vol. 178, S. Albonetti, S. Perathoner, and E. A. Quadrelli, Eds. Elsevier, 2019, pp. 65–84. doi: https://doi.org/10.1016/B978-0-444-64127-4.00004-5.

[7] K. Murugesan *et al.*, "Catalytic reductive aminations using molecular hydrogen for synthesis of different kinds of amines," *Chem. Soc. Rev.*, vol. 49, no. 17, pp. 6273–6328, 2020, doi: 10.1039/C9CS00286C.

[8] B. Emonts *et al.*, "Flexible sector coupling with hydrogen: A climate-friendly fuel supply for road transport," *Int. J. Hydrogen Energy*, vol. 44, no. 26, pp. 12918–12930, 2019, doi: 10.1016/j.ijhydene.2019.03.183.

[9] J. Choi, N. Hur, S. Kang, E. D. Lee, and K. B. Lee, "A CFD simulation of hydrogen dispersion for the hydrogen leakage from a fuel cell vehicle in an underground parking garage," *Int. J. Hydrogen Energy*, vol. 38, no. 19, pp. 8084–8091, 2013, doi: 10.1016/j.ijhydene.2013.02.018.

[10] E. G. Merilo, M. A. Groethe, J. D. Colton, and S. Chiba, "Experimental study of hydrogen release accidents in a vehicle garage," *Int. J. Hydrogen Energy*, vol. 36, no. 3, pp. 2436–2444, 2011, doi: 10.1016/j.ijhydene.2010.04.056.

[11] J. Beaucourt, G. Georgescu, J. Beaucourt, G. Georgescu, M. Hydrogen, and L. Psa, "Modelling Hydrogen Explosion in Level 1 PSA To cite this version : HAL Id : hal-03164341 Modeling hydrogen explosion in level 1 PSA," 2021.

[12] T. Gelain and C. Prévost, "Experimental and numerical study of light gas dispersion in a ventilated room," *Nucl. Eng. Des.*, vol. 293, pp. 476–484, 2015, doi: 10.1016/j.nucengdes.2015.07.059.

[13] J. Taveau, "Explosion hazards related to hydrogen releases in nuclear facilities," *J. Loss Prev. Process Ind.*, vol. 24, no. 1, pp. 8–18, 2011, doi: 10.1016/j.jlp.2010.08.002.

[14] L. Ricciardi, C. Prévost, L. Bouilloux, and R. Sestier-Carlin, "Experimental and numerical study of heavy gas dispersion in a ventilated room," *J. Hazard. Mater.*, vol. 152, no. 2, pp. 493–505, 2008, doi: 10.1016/j.jhazmat.2007.07.034.

© 2023 by JSME